applied sciences

MDPI

Article

Numerical Investigation of High-Purity Polarization-Entangled Photon-Pair Generation in Non-Poled KTP Isomorphs

Ilhwan Kim, Donghwa Lee and Kwang Jo Lee *

Department of Applied Physics, Institute of Natural Science, Kyung Hee University, Yongin-si 17104, Korea; dlfghks383@gmail.com (I.K.); fairytale095@gmail.com (D.L.)
* Correspondence: kjlee88@khu.ac.kr

Abstract: We investigated the high-purity entangled photon-pair generation in five kinds of "non-poled" potassium titanyl phosphate (KTP) isomorphs (i.e., $KTiOPO_4$, $RbTiOPO_4$, $KTiOAsO_4$, $RbTiOAsO_4$, and $CsTiOAsO_4$). The technique is based on the spontaneous parametric down-conversion (SPDC) under Type II extended phase matching (EPM), where the phase matching and the group velocity matching are simultaneously achieved between the interacting photons in non-poled crystals rather than periodically poled (PP) KTPs that are widely used for quantum experiments. We discussed both theoretically and numerically all aspects required to generate photon pairs in non-poled KTP isomorphs, in terms of the range of the beam propagation direction (or the spectral range of photons) and the corresponding effective nonlinearities and beam walk-offs. We showed that the SPDC efficiency can be increased in non-poled KTP isomorphs by 29% to 77% compared to PPKTP cases. The joint spectral analyses showed that photon pairs can be generated with high purities of 0.995–0.997 with proper pump filtering. In contrast to the PPKTP case, where the EPM is achieved only at one specific wavelength, the spectral position of photon pairs in the non-poled KTP isomorphs can be chosen over the wide range of 1883.8–2068.1 nm.

Keywords: parametric down-conversion; photon-pair generation; extended phase matching; potassium titanyl phosphate

Citation: Kim, I.; Lee, D.; Lee, K.J. Numerical Investigation of High-Purity Polarization-Entangled Photon-Pair Generation in Non-Poled KTP Isomorphs. *Appl. Sci.* **2021**, *11*, 565. https://doi.org/10.3390/app11020565

Received: 4 December 2020
Accepted: 7 January 2021
Published: 8 January 2021

1. Introduction

Spontaneous parametric down-conversion (SPDC) in second-order ($\chi^{(2)}$) nonlinear optic media has been a practical source of entangled quantum systems, especially due to its high stability [1,2]. In particular, two photons generated simultaneously via Type II SPDC have orthogonal polarizations in the basis that is distinguished by crystallographic axes, thus directly implementing a polarization-entangled photon-pair source. Several $\chi^{(2)}$ crystals, such as β-barium borate (β-BaB_2O_4, BBO), bismuth triborate (BiB_3O_6, BiBO), and periodically poled (PP) potassium titanyl phosphate ($KTiOPO_4$, KTP), have been utilized as material platforms for the implementation of Type II SPDC-based photon-pair sources [3–5]. Among these, PPKTP has attractive advantages over other crystals: (1) improvement of SPDC efficiency by using longer crystals than other cases under the collinear quasi-phase matching (QPM); (2) for Type II interaction, higher effective nonlinearity than other cases; and (3) most importantly, the generation of high-purity polarization-entangled photon pairs in the telecom C-band through the extended phase matching (EPM) [6–10]. In particular, "PPKTP Sagnac-loop" type SPDC sources have been used to demonstrate many quantum information experiments [9,10]. However, PPKTP requires sophisticated fabrication techniques, and despite the mature technology level, it is still challenging to form uniform-period PP structures in long-length KTP crystals. In addition, the actual thickness of PPKTP that can be manufactured by the electric poling method is limited to ~0.5 mm, due to the high electric conductivity of KTPs [11]. A higher voltage must be applied to the crystal to fabricate a thicker PPKTP, but if the voltage value required

for periodic poling exceeds the limit, the crystal burns or breaks during the fabrication. Although the PPKTP is still an attractive source of entangled quantum systems with the high spectral purity of photon pairs, Type II SPDC is also possible even without PP structures since non-poled KTPs are biaxial birefringent crystals. In addition, the effective nonlinear optic coefficients of KTP in the direction of crystallographic axes are larger than that of BBO or BiBO. Therefore, it is necessary to investigate whether the generation of high-purity photon pairs through Type II EPM is still possible and useful for practical quantum systems, even without the PP structure in KTP. To the best of our knowledge, no studies have been reported on SPDC-based photon-pair sources under Type II EPM in non-poled KTP isomorphs.

In this paper, we investigate both theoretically and numerically the high-purity polarization-entangled photon-pair generation in five kinds of non-poled KTP isomorphs—KTP, $KTiOAsO_4$ (KTA), $RbTiOPO_4$ (RTP), $RbTiOAsO_4$ (RTA), and $CsTiOAsO_4$ (CTA). The technique relies on the SPDC under Type II EPM, where the phase matching and the group velocity (GV) matching are simultaneously achieved between the interacting photons in non-poled crystals rather than PP ones. First, we investigated Type II EPM characteristics of five non-poled KTP isomorphs, in terms of the range of the beam propagation direction (or the spectral range of photon pairs) and the corresponding effective nonlinearities and beam walk-offs. We showed that the SPDC efficiency can be increased in non-poled KTP isomorphs by 29% to 77% compared to PPKTP. The joint spectral analyses showed that photon pairs can be generated with high purities of 0.995–0.997 with proper pump filtering. In contrast to the PPKTP case, where the EPM is achieved only at one specific wavelength, the spectral position of a photon pair in the non-poled KTP isomorphs can be chosen over the wide range of 1883.8–2068.1 nm. This means that the photon-pair spectra can be flexibly chosen in the range of interest while maintaining the high spectral purity of the photon pairs generated via Type II EPM.

2. Material and Theories

KTP isomorphs are usually expressed by the formula $MTiOXO_4$, where M can be potassium (K), rubidium (Rb), or cesium (Cs), and X can be arsenic (As) or phosphorus (P) [12]. Here, combinations other than KTP, RTP, KTA, RTA, and CTA are not commonly used because, except for these five, the growth of large and homogeneous bulk crystals is very difficult [13]. The KTP isomorphs have point symmetry of orthorhombic mm2 and exhibit biaxial birefringence. Their crystallographic axes a, b, and c are all perpendicular to each other and correspond to the optical axes x, y, and z, respectively, as shown in Figure 1a. In this definition, the order of refractive-index magnitudes is given by $n_x < n_y < n_z$ [14]. A wave vector representing the direction of beam propagation is defined in the spherical coordinate shown in Figure 1a, as follows:

$$\vec{k} = (\sin\theta\cos\phi,\ \sin\theta\sin\phi,\ \cos\theta). \tag{1}$$

Here, φ and θ are the azimuthal and polar angles, respectively. For Type II SPDC, an input single photon (pump) with a frequency of 2ω generates a pair of photons (signal and idler) with the same frequency of ω that are orthogonally polarized to each other, as illustrated in Figure 1b.

When the light is incident into the crystal, the refractive indices (RIs) of two eigen polarization modes for the given $\vec{k}$-direction can be obtained by solving the Fresnel equation of the wave normal as follows [15],

$$n_{q\omega}^{(p)} = \sqrt{\frac{2}{-B_q \pm \sqrt{B_q^2 - 4C_q}}}, \tag{2}$$

where the definitions of parameters are:

$$B_q = -k_x^2(b_q + c_q) - k_y^2(a_q + c_q) - k_z^2(b_q + a_q), \tag{3}$$

$$C_q = k_x^2 b_q c_q + k_y^2 a_q c_q + b_q a_q k_z^2, \tag{4}$$

$$a_q = n_{q\omega,x},\ b_q = n_{q\omega,y},\ c_q = n_{q\omega,z}. \tag{5}$$

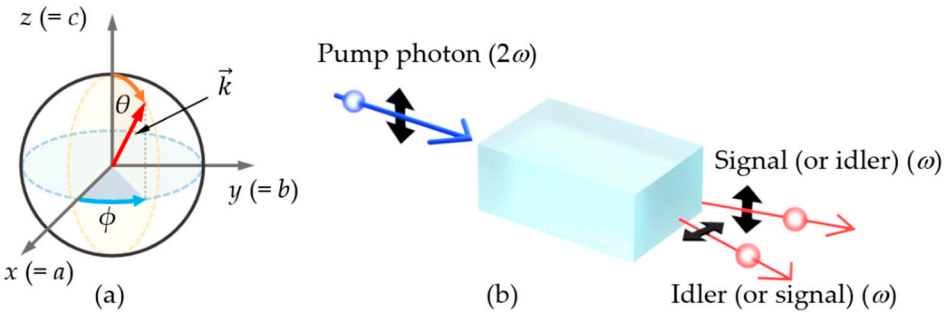

Figure 1. (**a**) A schematic diagram showing the definition of the crystallographic and optical axes of potassium titanyl phosphate (KTP) isomorphs in the spherical coordinate, where the wave vector, $\vec{k}$, represents the direction of beam propagation. φ and θ are the azimuthal and polar angles, respectively. (**b**) Type II spontaneous parametric down-conversion (SPDC): an input single photon (pump) with a frequency of 2ω generates a pair of photons (signal and idler) with the same frequency of ω that are orthogonally polarized to each other.

Here, q can be 1 or 2, then in the frequency-degenerate SPDC process, $n_{2\omega}$ and n_ω represent the RIs of pump photon with the frequency 2ω and signal (or idler) photon with the identical frequency ω, respectively. k_x, k_y, and k_z in Equations (3) and (4) are defined in Equation (1). p in Equation (2) can be h or l, representing high or low RI. Each of these corresponds to when taking minus and plus in the $\pm$ symbol of the denominator in Equation (2). The RIs of all 5 KTP isomorphs (i.e., n_x, n_y, and n_z) in Equation (5) are found in [16–19].

When photons of different frequencies pass through the crystal, a temporal walk-off (ΔT) between the interacting photons occurs due to their difference in GV. This GV mismatch is defined as ΔT per unit crystal length as follows,

$$\frac{\Delta T}{L} = \frac{\Delta n_g}{c}, \tag{6}$$

where L, c, and Δn_g represent the crystal length, the speed of light in vacuum, and the group index difference between interacting photons, respectively. Therefore, when $\Delta n_g = 0$, the GV matching is satisfied. Since the phase-matching (PM) condition between the pump, signal, and idler photons is given by $k_p = k_s + k_i$, the PM and GV matching conditions for Type II SPDC can be simplified as:

$$2n_{2\omega}^{(l)} = n_\omega^{(h)} + n_\omega^{(l)}, \tag{7}$$

$$2n_{g,2\omega}^{(l)} = n_{g,\omega}^{(h)} + n_{g,\omega}^{(l)}. \tag{8}$$

Now Type II EPM conditions are defined as when Equations (7) and (8) are satisfied simultaneously. Each of the equations is a 3-variable function for pump wavelength (λ_p), θ, and φ, thus by solving a system of equations (i.e., Equations (7) and (8)) for a given λ_p, we can find a set of θ and φ, i.e., the direction of $\vec{k}$. Thus, by sweeping $\vec{k}$ in the range of directions where the set of solutions exists, it is possible to continuously tune the resonant wavelength of the pump that produces pure biphoton states. This means that the spectral

position of the photon pair can be selectively determined or tuned in the range of interest. In contrast, in the cases of PPKTPs or bulk uniaxial crystals (e.g., β-BaB_2O_4 and $LiNbO_3$) that are widely used in quantum experiments, the EPM is satisfied only at one wavelength.

The mm2 crystals such as KTP isomorphs show biaxial birefringence. When the crystallographic axes and the optical axes have the relationships of $x = a$, $y = b$, and $z = c$, the effective nonlinearity for Type II interaction is generally expressed as [20],

$$d_{eff} = \xi_1 d_{15} + \xi_2 d_{24} + \xi_3 d_{31} + \xi_4 d_{32} + \xi_5 d_{33}, \tag{9}$$

where the nonlinear optic coefficients (d_{15}, d_{31}, d_{24}, d_{32}, and d_{33}) of 5 KTP isomorphs are listed in Table 1 with their references [21,22]. Under the relationships of $x = a$, $y = b$, and $z = c$, the ξ-coefficients in Equation (9) are given as follows:

$$\begin{aligned}
\xi_1 &= -AH(BEG + CH)^2 - AE(BGH - CE)(BEG + CH),\\
\xi_2 &= -AH(BCE - GH)^2 - AE(BCE - GH)(BCH + EG),\\
\xi_3 &= -AE(BGH - CE)(BEG + CH),\\
\xi_4 &= -AE(BCE - GH)(BCH + EG),\\
\xi_5 &= -A^3E^2H,
\end{aligned} \tag{10}$$

where the angle-dependent parameters of A, B, C, G, E, and H are given by $\sin\theta$, $\cos\theta$, $\sin\varphi$, $\cos\varphi$, $\sin\delta$, and $\cos\delta$, respectively. θ and φ are the angles defined in Figure 1a. δ is an angle introduced only for convenience and is defined as:

$$\tan\delta \equiv \frac{2BCG}{A^2\cot^2 V_z + C^2 - B^2G^2}, \tag{11}$$

where V_z represents the angle between the z-axis and the optic axis of biaxial birefringence when the relation of $n_x < n_y < n_z$ is valid, as in the case of KTP isomorphs. V_z is related to Sellmeier equations of the crystal [20]. Therefore, d_{eff} is also a 3-variable function for λ_p, θ, and φ, and thus can be obtained by substituting the solution sets of λ_p, θ, and φ that satisfy Type II EPM (i.e., Equations (7) and (8)). The SPDC efficiency is proportional to the square of the d_{eff} coefficient for a given k_p-direction [23].

Table 1. Non-zero nonlinear optic coefficients of 5 KTP isomorphs at 1064 nm (in pm/V).

Crystals	d_{15}	d_{31}	d_{24}	d_{32}	d_{33}
KTP [21]	2.02 ± 0.15	2.01 ± 0.07	3.75 ± 0.07	3.75 ± 0.07	15.4 ± 0.2
RTP [21]	1.98 ± 0.34	2.05 ± 0.07	3.98 ± 0.39	3.82 ± 0.1	15.6 ± 0.3
RTA [21]	2.17 ± 0.20	2.25 ± 0.07	3.92 ± 0.15	3.89 ± 0.08	15.9 ± 0.3
KTA [21]	2.30 ± 0.05	2.30 ± 0.05	3.64 ± 0.34	3.66 ± 0.08	15.5 ± 0.3
CTA [22]	2.1 ± 0.4 [1]	2.1 ± 0.4	3.4 ± 0.7 [1]	3.4 ± 0.7	18.1 ± 1.8

[1] Reasonably, assuming that Kleinman symmetry is valid, $d_{24} = d_{32}$ and $d_{15} = d_{31}$.

When the interacting beams pass through a birefringent crystal, the spatial walk-off between the beams occurs due to the difference between $\vec{k}$ and $\vec{s}$ (Poynting vector) directions in the crystal. In biaxial birefringent crystals, the angle $\rho_q^{(p)}$ between $\vec{k}$ and $\vec{s}$ is given by,

$$\tan\rho_q^{(p)} \equiv \left\{n_{q\omega}^{(p)}\right\}^2 \left[\left(\frac{k_x}{\left\{n_{q\omega}^{(p)}\right\}^{-2} - a_q}\right)^2 + \left(\frac{k_y}{\left\{n_{q\omega}^{(p)}\right\}^{-2} - b_q}\right)^2 + \left(\frac{k_z}{\left\{n_{q\omega}^{(p)}\right\}^{-2} - c_q}\right)^2\right]^{-1/2}, \tag{12}$$

where all parameters of Equation (12) are defined in Equations (1)–(5). For Type II EPM, the low-RI signal (or idler) beam ($\rho_1^{(l)}$) is always placed between the low-RI pump beam ($\rho_2^{(l)}$) and the high-RI idler (or signal) beam ($\rho_1^{(h)}$), as can be seen from Equation (7) [24]. In

this case, the walk-off angle w can be defined as the largest angle between the Poynting vectors of the interacting photons:

$$\cos w = \cos \rho_1^{(h)} \cos \rho_2^{(l)}. \tag{13}$$

As expected in Equation (13), w is also the 3-variable function for λ_p, θ, and φ, which can be obtained by substituting the set of solutions of λ_p, θ, and φ that satisfies Type II EPM. Then the maximum deviation between the interacting beams after passing through a crystal of length L can be expressed as:

$$\Delta = L \tan w. \tag{14}$$

The construction of the signal-idler joint spectral amplitude (JSA) and the calculation of the purity of biphoton state via Schmidt decomposition is a good way to quantify the heralded-state spectral purity of SPDC output. The biphoton state $|\psi\rangle$ generated from SPDC can be expressed as,

$$|\psi\rangle = \int_0^\infty \int_0^\infty d\omega_s d\omega_i f(\omega_s, \omega_i) \hat{a}_s^\dagger(\omega_s) \hat{a}_i^\dagger(\omega_i) |0\rangle |0\rangle, \tag{15}$$

where $\hat{a}_s^\dagger$ and $\hat{a}_i^\dagger$ denote the creation operators of the signal and idler photons, respectively, and ω_s and ω_i are the corresponding frequencies [25]. Here, the normalized correlation function $f(\omega_s, \omega_i)$, representing the biphoton JSA, is expressed as the product of pump envelop function and the PM function as follows:

$$f(\omega_s, \omega_i) = \alpha(\omega_s, \omega_i) \varphi(\omega_s, \omega_i). \tag{16}$$

Assuming a pump with Gaussian spectral shape, the pump envelope (PE) function can be written as,

$$\alpha(\omega_s, \omega_i) \propto \exp\left[-\frac{(\omega_s + \omega_i - \omega_p)^2}{\sigma_p^2} \right], \tag{17}$$

where ω_p and σ_p represent the center frequency and bandwidth of the pump, respectively. The PM function is given in the form of a sinc function as shown below,

$$\varphi(\omega_s, \omega_i) \propto \operatorname{sinc}\left(\frac{\Delta k L}{2} \right), \tag{18}$$

where Δk represents the phase mismatch defined as $\Delta k = |k_p - k_s - k_i|$. For the given k_p-direction (i.e., θ and φ) that satisfies the EPM, Equation (16) is given as a function of the signal and idler wavelengths (or λ_s and λ_i), thus the JSA can be plotted on a two-dimensional plane as a function of λ_s and λ_i. The purity can be calculated via the following Schmidt decomposition related to Equation (15),

$$f(\omega_s, \omega_i) = \sum_j \sqrt{c_j} \left| \zeta_{s,j} \right\rangle \left| \zeta_{i,j} \right\rangle, \tag{19}$$

where Schmidt coefficients, c_j, denote a set of non-negative real numbers satisfying the normalization condition, $\sum_j c_j = 1$. $\left| \zeta_{s,j} \right\rangle$ and $\left| \zeta_{i,j} \right\rangle$ represent the orthonormal basis states (i.e., Schmidt modes), respectively. Then the purity, P, is defined as the sum of squares of Schmidt coefficients as [25]:

$$P = \sum_j c_j^2. \tag{20}$$

Therefore, once we plot the JSA as a function of λ_s and λ_i in a 2-dimensional plane, P can be calculated via the Schmidt decomposition in Equation (20).

3. Simulations and Discussion

Figure 2 shows the numerical simulation results of the PM and GV matching for Type II EPM: Figure 2a–e correspond to KTP, RTP, RTA, KTA, and CTA in turn. In each graph, the blue and cyan surfaces represent the PM and GV matching calculated using Equations (7) and (8), respectively. The crossing line of two surfaces means the range of $\vec{k}$-direction (i.e., θ and φ) satisfying the EPM, which spans a specific wavelength region as expected in Section 2. Figure 3 plots θ and φ as a function of the resonant λ_p, corresponding to the crossing lines in Figure 2. Figure 3a–e correspond to KTP, RTP, RTA, KTA, and CTA, respectively, as in Figure 2. For each KTP isomorph, Type II EPM is possible for all azimuthal angles (φ = 0–90°), whereas for polar angles (θ) only in a specific angular region as plotted in Figure 3. Type II EPM properties calculated for all five crystals are summarized in Table 2 with the references to Sellmeier equations used for the simulations [16–19]. The spectral ranges of the entangled photon pairs calculated for all five crystals span 1883.8–2068.1 nm, which is still within the silica fiber transparency (e.g., SM2000, 1700 nm to 2300 nm, Thorlabs) [26]. Therefore, quantum light sources based on KTP isomorphs have good potential for quantum communication in the sense that the existing optical communication infrastructure can be used almost as it is. In addition, since absorption lines of various gas molecules (e.g., hydrogen chloride (HCl), ammonium (NH_3), water vapor (H_2O), carbon dioxide (CO_2), and nitrous oxide (N_2O)) exist in this spectral region, the KTP isomorph-based quantum light sources can be exploited in sensing applications [27]. The spectral ranges of the photon pairs, which can be tuned by sweeping the direction of k_p, reach tens of nm as listed in Table 2, which provides flexibility in choosing the wavelength of the quantum light source while maintaining the high spectral purity.

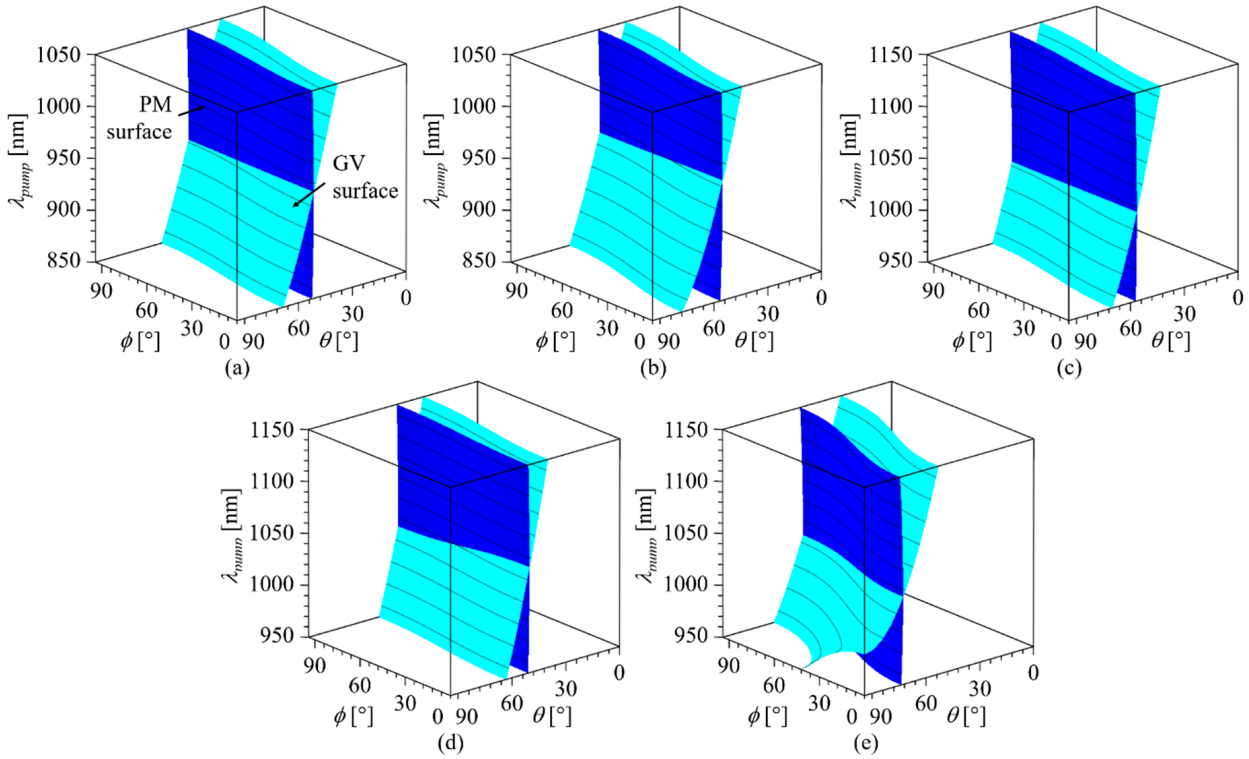

Figure 2. Numerical simulation results of the phase matching (PM) and group velocity (GV) matching for Type II extended phase matching (EPM): (**a**) KTP, (**b**) RTP, (**c**) RTA, (**d**) KTA, and (**e**) CTA. In each graph, the blue and cyan surfaces represent the PM and GV matching, respectively. The crossing line of two surfaces means the range of k_p-direction satisfying the EPM.

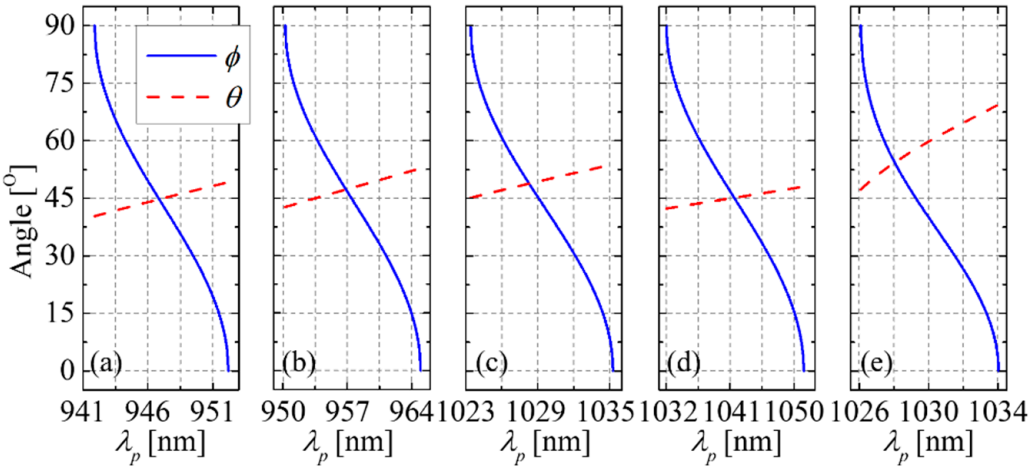

Figure 3. k-directions (φ and θ) for Type II EPM and the corresponding resonant pump wavelength (λ_p). The EPM is possible for all azimuthal angles (φ = 0–90°), whereas for polar angles (θ), only in a specific angular region: (**a**) KTP, (**b**) RTP, (**c**) RTA, (**d**) KTA, and (**e**) CTA.

Table 2. $\vec{k}$ -direction and wavelength ranges of the interacting photons satisfying Type II EPM.

Crystals	φ [°]	θ [°]	λ_p [nm]	λ_s (or λ_i) [nm]	$\Delta\lambda_s$ (or $\Delta\lambda_i$) [nm]
KTP [16]	0–90	40.3–49.2	941.9–952.2	1883.8–1904.4	20.6
RTP [19]	0–90	42.7–52.8	950.3–965.0	1900.5–1930.0	29.4
RTA [18]	0–90	45.1–53.9	1023.4–1035.3	2046.8–2070.5	23.7
KTA [17]	0–90	42.3–48.1	1032.0–1051.4	2064.0–2102.8	38.8
CTA [17]	0–90	47.3–69.4	1026.1–1034.0	2052.2–2068.1	15.9

Since the SPDC efficiency is proportional to the square of d_{eff}, it is critical to estimate the effective nonlinearity for the given $\vec{k}$-direction that satisfies the EPM. Figure 4 shows the d_{eff} values plotted as a function of λ_p, which are calculated numerically using Equation (9). The λ_p values in the horizontal axes in Figure 4 correspond to the λ_p range of Type II EPM listed in Table 2. For each case, the d_{eff} value is larger at longer wavelengths under Type II EPM. The maximum d_{eff} values are obtained at φ = 0 for all five crystals (i.e., the case that k_p lies on the x-z plane shown in Figure 1a). These d_{eff} values at φ = 0 and their corresponding polar angles θ and resonant λ_p's are listed in Table 3. In the PPKTP case, the nonlinear optic coefficient (d_{QPM}) is given as $(2/\pi)d_{24}$ for the first-order QPM. The simulation results show that the d_{eff} values are larger for non-poled crystals (2.71–3.18) than for PPKTP (2.39). The ratios of d_{QPM} to the d_{eff} values of the non-poled KTP isomorphs are summarized in Table 3. Since the SPDC efficiency is proportional to the square of d_{eff}, $(d_{eff}/d_{QPM})^2$ represents the ratio of efficiency that can be increased for each case compared to the case of PPKTP. As shown in Table 3, the SPDC efficiency is expected to be improved as much as from 29% to 77% in a quantum light source using non-poled KTP isomorphs.

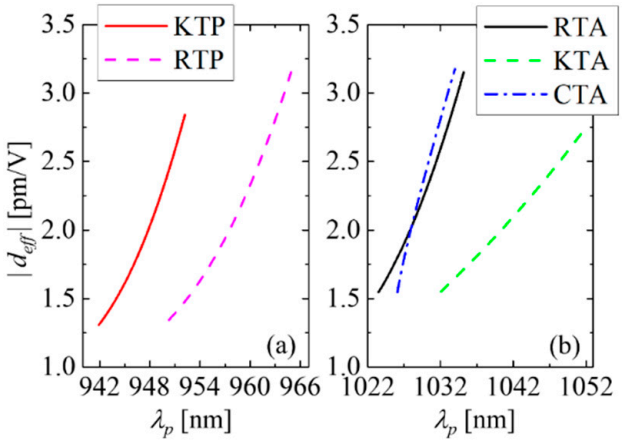

Figure 4. Effective nonlinear optic coefficients (d_{eff}) calculated numerically under Type II EPM: (**a**) KTP and RTP; (**b**) RTA, KTA, and CTA.

Table 3. Type II EPM conditions for the maximum effective nonlinearities: the resonant pump wavelength (λ_p), the *k*-direction (i.e., θ and φ), the effective nonlinear optic coefficient (d_{eff}), the walk-off angle (w), and the beam deviation (Δ).

Crystals	λ_p [nm]	φ [°]	θ [°]	d_{eff} [pm/V]	$(d_{eff}/d_{QPM})^2$	w [°]	Δ [μm/mm]
KTP	952.19	0	49.2	2.80	1.37	2.8	48.9
RTP	964.98	0	52.8	3.17	1.76	2.7	47.2
RTA	1035.27	0	53.9	3.17	1.76	2.2	38.4
KTA	1051.40	0	48.1	2.71	1.29	2.3	40.2
CTA	1034.04	0	69.4	3.18	1.77	1.9	33.2
PPKTP	775	0	90	2.39 [1]	1	-	-

[1] $d_{QPM} = (2/\pi)d_{24}$, the first-order quasi-phase matching (QPM).

Figure 5 shows the walk-off angles (w) calculated using Equation (13) under Type II EPM: (a) KTP and RTP and (b) RTA, KTA, and CTA plotted as a function of the EPM λ_p values. Over the whole range of λ_p, the calculated w spans 1.6–2.8° for the five crystals. The corresponding beam deviation (Δ) per unit millimeter crystal length calculated using Equation (14) spans 27.9–48.9 μm/mm, which can be sufficiently overcome by a large beam window in thick crystals. In each crystal, the calculated values of w and Δ for the case with the maximum d_{eff} value are also summarized in Table 3.

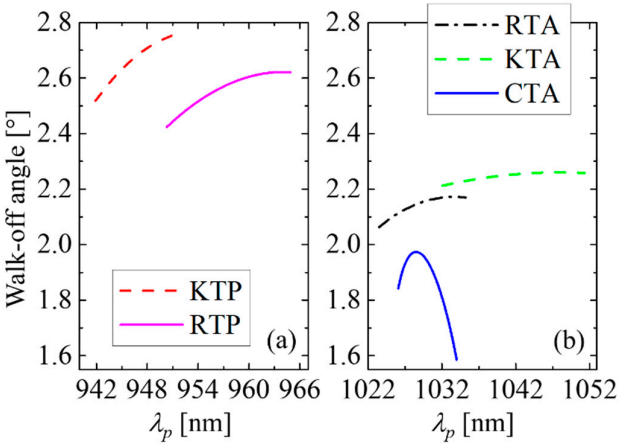

Figure 5. Walk-off angle (w) between the interacting beams numerically calculated under Type II EPM: (**a**) KTP and RTP; (**b**) RTA, KTA, and CTA.

In order to quantify the heralded-state spectral purity of SPDC output, we analyzed the signal-idler JSA properties and calculated the purity of the biphoton state. Figure 6 shows the joint spectral properties of Type II SPDC in the non-poled KTP with the largest d_{eff} shown in Table 3. Note that in this case, k_p lies on the x-z plane (i.e., $\varphi = 0$ in Figure 1a), thus the optical alignment is relatively easy compared to the other cases for $\varphi \neq 0$ (Table 2). The density plot of the PM function (Figure 6b) shows typical EPM characteristics as in the PPKTP case [10]. The joint spectral intensity (JSI) calculated for the 3.3-nm bandwidth PE function (Figure 6a) is plotted in Figure 6c. Here, the crystal length of 10 mm is used for calculations, and the JSI is defined as $|\mathrm{JSA}|^2$. The solid and dashed lines in Figure 6d represent the contour lines for JSI = 0.5 and a circle with a diameter of 11 nm, respectively. The contour line shows a circular shape, and the purity calculated using Schmidt decomposition in Equation (20) is as high as 0.996.

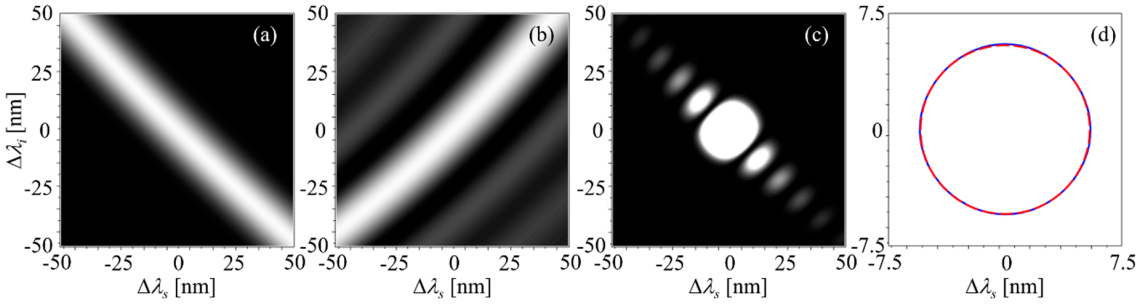

Figure 6. Type II SPDC in a non-poled KTP with the maximum d_{eff} (Table 1) (**a**) pump envelope (PE) function, (**b**) PM function, (**c**) joint spectral intensity (JSI), and (**d**) the contour line for JSI = 0.5 (blue solid line) shown with a circle with a diameter of 11 nm (red dashed line). The calculated purity is 0.996.

Figure 7 shows the JSIs of Type II SPDC in non-poled RTP, RTA, KTA, and CTA with maximum d_{eff} values (Table 3), where the PE functions of 2.2-nm, 4.05-nm, 4.05-nm, and 3.0-nm bandwidth, respectively, were considered for higher purities. The contours of JSI = 0.5 (blue solid line) for each case shown in Figure 7 are plotted in Figure 8. The red dashed lines shown in Figure 8 represent the circles with diameters of 7.35 nm, 13.6 nm, 13.6 nm, and 10 nm, respectively. All calculation results in Figures 7 and 8 were performed for 10-mm crystal length. To clearly compare the spectral bandwidths of the photon pairs, all density plots in Figures 6 and 7 are displayed in a window with the size set to 100 nm × 100 nm, and Figures 6d and 8 are displayed in a 15 nm × 15 nm window. As shown in Figure 8, the contours of JSI = 0.5 exhibit circular shapes for all five crystals, and the calculated spectral purities are 0.997 for RTP and 0.995 for RTA, KTA, and CTA, respectively. This means that very high-purity entangled photon pairs can be generated in five non-poled bulk KTP isomorphs, as well as in the case of the well-known PPKTP [10]. In addition, in terms of SPDC efficiency, all five non-poled KTP isomorphs discussed in this study show advantages over the case of PPKTP using the first-order QPM, as discussed in Table 3.

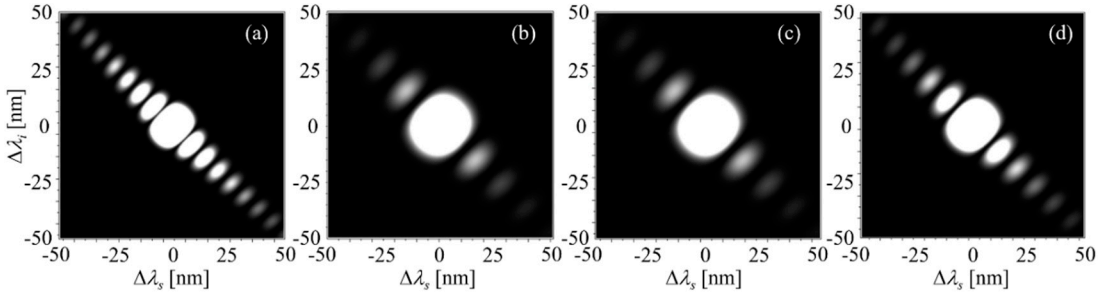

Figure 7. JSIs of Type II SPDC in non-poled (**a**) RTP, (**b**) RTA, (**c**) KTA, and (**d**) CTA with maximum d_{eff} values (Table 3). The calculated purities are 0.997, 0.995, 0.995, and 0.995, respectively.

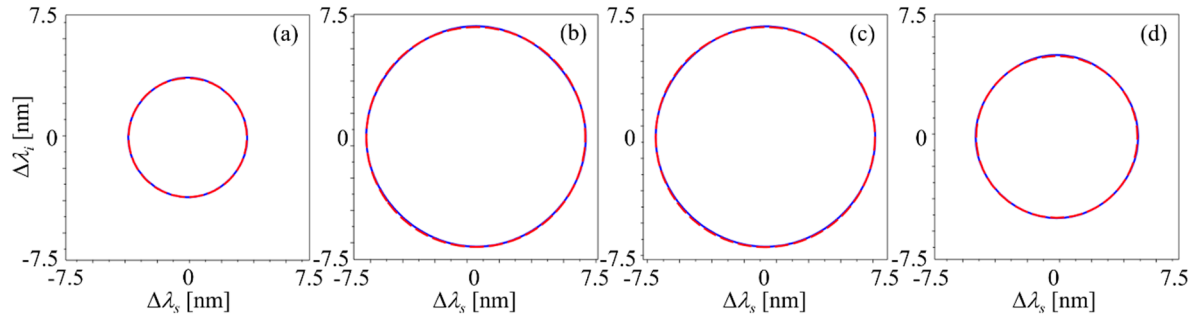

Figure 8. Contour lines for JSI = 0.5 (blue solid lines) for the cases shown in Figure 7: (**a**) RTP, (**b**) RTA, (**c**) KTA, and (**d**) CTA. The red dashed lines represent the circles with diameters of 7.35 nm, 13.6 nm, 13.6 nm, and 10 nm, respectively. Each result was calculated for a crystal length of 10 mm.

4. Conclusions

We theoretically and numerically investigated the entangled photon-pair generation in five kinds of non-poled KTP isomorphs: KTP, RTP, RTA, KTA, and CTA. The SPDC properties under Type II EPM were theoretically investigated in the mm2 biaxial crystal to which the KTP isomorphs belong, including PM, GV matchings, effective nonlinearities, and spatial walk-offs between the interacting photons. The heralded-state spectral purities of SPDC output were quantified via JSA analyses, and the results show that the purities calculated for Type II EPM with a proper pump filtering are as high as 0.995–0.997. The spectral position of photon-pairs produced by KTP isomorphs can be chosen over the broad range of 1883.8–2068.1 nm, which is still within the silica fiber transparency. Therefore, the spectral position of the photon pair can be selectively determined or tuned in the range of interest while maintaining the high spectral purity of the photon pairs generated via Type II EPM. In addition, the use of non-poled crystals is expected to increase the SPDC efficiency by 29% to 77% compared to the PPKTP. Since KTP isomorphs have been commercialized as high-level crystal growth techniques, quantum light sources based on non-poled KTP isomorphs have good potential for fiber-optic and free-space quantum communication and sensing.

Author Contributions: Conceptualization, K.J.L.; Simulation, D.L.; writing—original draft preparation, I.K.; writing—review and editing, K.J.L.; supervision, K.J.L. All authors have read and agreed to the published version of the manuscript.

Funding: This research was funded by the National Research Foundation of Korea (Grant NRF-2019R1F1A1063937) and by the Korea Institute of Science and Technology (KIST) (Grant 2E29580-19-147).

Institutional Review Board Statement: Not applicable.

Informed Consent Statement: Not applicable.

Data Availability Statement: The data presented in this study are available in this article.

Conflicts of Interest: The authors declare no conflict of interest.

References

1. Alber, G.; Beth, T.; Horodecki, M.; Horodecki, P.; Horodecki, R.; Rötteler, M.; Weinfurter, H.; Werner, R.; Zeilinger, A. *Quantum Information*; Springer: Berlin, Germany, 2001; pp. 74–79.
2. Bouwmeester, D.; Zeilinger, A. *The Physics of Quantum Information: Basic Concepts*; Springer: Berlin, Germany, 2000; pp. 1–14.
3. Kwiat, P.; Mattle, K.; Weinfurter, H.; Zeilinger, A.; Sergienko, A.V.; Shih, Y. New High-Intensity Source of Polarization-Entangled Photon Pairs. *Phys. Rev. Lett.* **1995**, *75*, 4337–4341. [CrossRef] [PubMed]
4. Halevy, A.; Megidish, E.; Dovrat, L.; Eisenberg, H.; Becker, P.; Bohatý, L. The biaxial nonlinear crystal BiB_3O_6 as a polarization entangled photon source using non-collinear type-II parametric down-conversion. *Opt. Express* **2011**, *19*, 20420. [CrossRef] [PubMed]

5. Steinlechner, F.; Gilaberte, M.; Jofre, M.; Scheidl, T.; Torres, J.P.; Pruneri, V.; Ursin, R. Efficient heralding of polarization-entangled photons from type-0 and type-II spontaneous parametric downconversion in periodically poled $KTiOPO_4$. *J. Opt. Soc. Am. B* **2014**, *31*, 2068–2076. [CrossRef]
6. Giovannetti, V.; Maccone, L.; Shapiro, J.H.; Wong, F.N. Generating Entangled Two-Photon States with Coincident Frequencies. *Phys. Rev. Lett.* **2002**, *88*, 183602. [CrossRef] [PubMed]
7. Giovannetti, V.; Maccone, L.; Shapiro, J.H.; Wong, F.N. Extended phase-matching conditions for improved entanglement generation. *Phys. Rev. A* **2002**, *66*, 043813. [CrossRef]
8. Jin, R.-B.; Shimizu, R.; Wakui, K.; Fujiwara, M.; Yamashita, T.; Miki, S.; Terai, H.; Wang, Z.; Sasaki, M. Pulsed Sagnac polarization-entangled photon source with a PPKTP crystal at telecom wavelength. *Opt. Express* **2014**, *22*, 11498–11507. [CrossRef] [PubMed]
9. Li, Y.; Zhou, Z.-Y.; Ding, D.-S.; Shi, B.-S. CW-pumped telecom band polarization entangled photon pair generation in a Sagnac interferometer. *Opt. Express* **2015**, *23*, 28792–28800. [CrossRef] [PubMed]
10. Weston, M.M.; Chrzanowski, H.M.; Wollmann, S.; Boston, A.; Ho, J.; Shalm, L.K.; Verma, V.B.; Allman, M.S.; Nam, S.W.; Patel, R.B.; et al. Efficient and pure femtosecond-pulse-length source of polarization-entangled photons. *Opt. Express* **2016**, *24*, 10869–10879. [CrossRef] [PubMed]
11. Raicol Crystals Ltd. Available online: https://raicol.com (accessed on 21 November 2020).
12. Bierlein, J.D.; Vanherzeele, H. Potassium titanyl phosphate: Properties and new applications. *J. Opt. Soc. Am. B* **1989**, *6*, 622. [CrossRef]
13. Stolzenberger, R.A.; Scripsick, M.P. Recent advancements in the periodic poling and characterization of RTA and its isomorphs. *Proc. SPIE* **1999**, *3610*, 23–35. [CrossRef]
14. Dmitriev, V.G.; Gurzadyan, G.G.; Nikogosyan, D.N. *Handbook of Nonlinear Optical Crystals*, 3rd ed.; Springer: Berlin/Heidelberg, Germany, 1999; pp. 107–108.
15. Yariv, A.; Yeh, P. *Photonics: Optical Electronics in Modern Communications*, 6th ed.; Oxford University Press: New York, NY, USA, 2007; pp. 30–33.
16. Kato, K.; Takaoka, E. Sellmeier and thermo-optic dispersion formulas for KTP. *Appl. Opt.* **2002**, *41*, 5040–5044. [CrossRef] [PubMed]
17. Fève, J.-P.; Boulanger, B.; Pacaud, O.; Rousseau, I.; Ménaert, B.; Marnier, G.; Villeval, P.; Bonnin, C.; LoIacono, G.M.; LoIacono, D.N. Phase-matching measurements and Sellmeier equations over the complete transparency range of $KTiOAsO_4$, $RbTiOAsO_4$, and $CsTiOAsO_4$. *J. Opt. Soc. Am. B* **2000**, *17*, 775–780. [CrossRef]
18. Kato, K.; Takaoka, E.; Umemura, N. Thermo-Optic Dispersion Formula for RbTiOAsO4. *Jpn. J. Appl. Phys.* **2003**, *42*, 6420–6423. [CrossRef]
19. Guillien, Y.; Ménaert, B.; Feve, J.; Segonds, P.; Douady, J.; Boulanger, B.; Pacaud, O. Crystal growth and refined Sellmeier equations over the complete transparency range of RbTiOPO4. *Opt. Mater.* **2003**, *22*, 155–162. [CrossRef]
20. Dmitriev, V.; Nikogosyan, D. Effective nonlinearity coefficients for three-wave interactions in biaxial crystal of mm2 point group symmetry. *Opt. Commun.* **1993**, *95*, 173–182. [CrossRef]
21. Pack, M.V.; Armstrong, D.J.; Smith, A.V. Measurement of the $\chi^{(2)}$ tensors of $KTiOPO_4$, $KTiOAsO_4$, $RbTiOPO_4$, and $RbTiOAsO_4$ crystals. *Appl. Opt.* **2004**, *43*, 3319–3323. [CrossRef] [PubMed]
22. Cheng, L.T.; Cheng, L.K.; Bierlein, J.D.; Zumsteg, F.C. Nonlinear optical and electro-optical properties of single crystal CsTiOAsO4. *Appl. Phys. Lett.* **1993**, *63*, 2618–2620. [CrossRef]
23. Boyd, R.W. *Nonlinear Optics*, 4th ed.; Academic Press: San Diego, CA, USA, 2020; pp. 70–73.
24. Brehat, F.; Wyncke, B. Calculation of double-refraction walk-off angle along the phase-matching directions in non-linear biaxial crystals. *J. Phys. B At. Mol. Opt. Phys.* **1989**, *22*, 1891–1898. [CrossRef]
25. Mosley, P.J.; Lundeen, J.S.; Smith, B.J.; Walmsley, I.A. Conditional preparation of single photons using parametric downconversion: A recipe for purity. *New J. Phys.* **2008**, *10*, 093011. [CrossRef]
26. Thorlabs Inc. Available online: https://www.thorlabs.com/thorproduct.cfm?partnumber=SM2000 (accessed on 15 November 2020).
27. Nanoplus GmbH. Available online: https://nanoplus.com/en/applications/applications-by-gas (accessed on 15 November 2020).